Marine and Petroleum Geology 64 (2015) 31–42

Contents lists available at ScienceDirect

Marine and Petroleum Geology

journal homepage: www.elsevier.com/locate/marpetgeo

Research paper

Subsea gas emissions from the Barbados Accretionary Complex

A. Barnard [a, *], W.W. Sager [a], J.E. Snow [a], M.D. Max [b]

[a] Department of Earth and Atmospheric Sciences, University of Houston, Houston, TX 77204, USA
[b] Hydrate Energy International, 612 Petit Berdot Drive, Kenner, LA 70065, USA

ARTICLE INFO

Article history:
Received 4 February 2015
Accepted 6 February 2015
Available online 17 February 2015

Keywords:
Barbados
Multibeam
Water column
Marine
Geology
Hydrate
Methane
Subsea

ABSTRACT

We have identified and analyzed the affect of newly identified gas plumes in the water column from the Barbados Accretionary Complex. Multibeam echo soundings from cruise AT21-02 acquired using a Kongsberg EM122 system were used to define a region with several ~600–900 m tall gas plumes in the water column directly above cratered hummocky regions of the sea floor having relatively high backscatter at a water depth of ~1500 m. The natural gas hydrate stability zone reaches a minimum depth of ~600 m in the water column, similar to that of the tallest imaged bubble plumes, which implies hydrate shells on the gas bubbles. Tilting of the plume shows current shear in the water column, with a current direction from the northwest to southeast at 128°, a direction similar to the transport direction of North Atlantic Deep Water in this region. The source of hydrocarbons, determined from existing geochemical data, suggests the gas source was subjacent marine Cretaceous source rocks. North–south trending faults, craters and mud volcanoes associated with the gas plumes point to the presence of a deep plumbing system and indicate that gas is a driver of mud volcanism in this region. The widespread occurrence of seafloor morphology related to venting indicates that subsea emissions from the Barbados Accretionary Complex are substantial.

1. Introduction

Near vertical acoustic anomalies in the water column, associated with gas rising from the seafloor and termed acoustic "flares" are commonly identified in echograms from sonar systems (Colbo et al., 2014 and references therein). Integration of bathymetry, backscatter and water column acoustic data by modern multibeam sonar processing software provides water column features with a geological context. Shipboard, remote and autonomous vehicle operated multibeam systems are well suited as detection sensors when trying to identify and evaluate the extent and number of natural emission sites present on the seafloor, as well as for identifying anthropogenic emissions (Weber et al., 2012; Wynn et al., 2014). Repeated survey sweeps enable a time dimension that can detect temporal changes. Water current displacement of gas plumes is commonly imaged within multibeam data and can help identify deep currents and aid in focusing seafloor studies to emission sources (Schneider et al., 2010).

Cold seeps consisting of gas and fluid most commonly vent from emission sites in marine sediments on continental shelves and slopes. They vary in their rate of effusion and temperature (almost always <30 °C) depending on their sources, transport distance, and mechanisms of ascent. Subsurface geology may determine the presence of a source, migration pathways, and the location of surface features (Riedel et al., 2002; Talukder, 2012; Talukder et al., 2007). At the seafloor, emission site morphology is a result of the gas releasing mechanisms, depth of the natural gas hydrate stability zone (GHSZ), and gas flux (Naudts et al., 2010; Roberts et al., 2006). Subsea gas and fluid emission sites can be identified by their effect on surface morphology, and the formation of pockmarks/craters (Brothers et al., 2012; Chand et al., 2009; King and MacLean, 1970; Pilcher and Argent, 2007; Tinivella and Giustiniani, 2012), mud volcanoes (Bonini, 2012; Jerosch et al., 2007; Kopf, 2002; Milkov, 2000; Sager et al., 2003; Savini et al., 2009; Van Rensbergen et al., 2002; Zitter et al., 2005), natural gas hydrate (NGH, which refers to any combination of hydrocarbon gases although dominantly methane) pingoes/mounds, (Haeckel et al., 2004; Paull et al., 2007; Serié et al., 2012; Simonetti et al., 2013; Van Dover et al., 2003), although these are less common, and authigenic carbonates (Aloisi et al., 2000; Bian et al., 2013; Bohrmann et al., 1998; Johnson et al., 2003). These seafloor

* Corresponding author. Tel.: +1 832 705 9223.
E-mail address: abarnard2@uh.edu (A. Barnard).

http://dx.doi.org/10.1016/j.marpetgeo.2015.02.008
0264-8172/

features not only provide a record of the surficial processes but they are also a key to diagenetic activity in the subsurface. For example, fault scarps on the seafloor may be a morphologically distinct part of the migration pathway that delivers gases, and fluids, from the lithosphere into the ocean, and potentially atmosphere.

Because of the gases and fluids released, emission sites play an important role in biological and chemical processes on the seafloor (Agirrezabala et al., 2012; Blackford et al., 2014; Cao et al., 2013; Hovland et al., 2012; Zemskaya et al., 2012). Bubble release activity, that is the volumetric and rate of gas release in natural systems varies (Greinert, 2008; Kannberg et al., 2013; Leifer et al., 2004: Leifer and MacDonald, 2003; Naudts et al., 2010; Nikolovska et al., 2008; Sauter et al., 2006; Torres et al., 2002), with the dominant control being changes in the source region and the degree of resistance to the upward force of buoyancy (Leifer et al., 2004). The pressure differential between the source and migration pathway may be great enough to rupture NGH seals (Daigle et al., 2011; Tryon et al., 2002, 1999).

Gas release activity is also influenced in shallow (<500 m) water by changes in source pressure due to currents and tides (Boles et al., 2001; Greinert et al., 2006; Linke et al., 2010; Newman et al., 2008; Torres et al., 2002). Continuous monitoring of a few sample emission sites is just beginning. 4-D monitoring would be necessary to provide a more complete picture of the temporal and volumetric variability of vent flow (Bayrakci et al., 2014).

The Intergovernmental Panel on Climate Change has estimated that natural emissions of methane into the atmosphere from faults, fractured rocks and the seafloor is 40–60 Tg yr^{-1}, or 15–20 % of global emissions, (Denman et al., 2007; Kvenvolden and Rogers, 2005) but there is a high degree of uncertainty in the location and clustering of emission site locations, numbers and volumes of gases involved. This is important because present-day atmospheric methane levels are higher than the past ~650 ka and increasing (Spahni et al., 2005; Nisbet et al., 2014). Estimates of NGH volumes on Earth and Mars (Max et al., 2013; Milkov, 2004) and the quantities of gas delivered into the oceans and atmosphere (Fisher et al., 2011; Leifer et al., 2004) from the subsurface vary widely. This leads to a high degree of uncertainty over the potential impact that NGH have on the climate system, and whether a proportion of the gases vented from the seafloor could be partly responsible for changes in the climate system observed during Earth's history, e.g., ocean acidification and intensification of greenhouse conditions (Dawson et al., 2011; Jones et al., 2010; Max et al., 2006; McGuire and Maslin, 2012; Phrampus and Hornbach, 2012; Skarke et al., 2014; Smith et al., 2014).

The GHSZ is the reservoir zone for unconventional NGH concentrations that sequester migrating, and *in-situ* (e.g., biogenic) gases and fluids (Max and Johnson, 2014) that might otherwise reach the seafloor. Release of the constituent gas and fresh water phases may occur when the gas trap beneath the GHSZ boundary is breached, for instance by faulting or sediment failure, Conversion of NGH will take place when seafloor warming reaches the lower part of the GHSZ or when sea level falls and pressure reduces. Failure of the trap integrity has been postulated from reflection seismic evidence to release large quantities of natural gas from the seafloor (Dillon et al., 2001).

The base of the GHSZ frequently appears in seismic data as an ocean bottom simulating reflector (BSR) with opposite polarity to that seen at the seafloor (Hyndman and Spence, 1992; Shipley et al., 1979). Prominent BSR indicates the presence of a low pressure wave free gas zone immediately below the GHSZ. Gas molecules within the GHSZ are presumed to be largely contained within solid NGH. The presence of BSR alone is not evidence for the existence of NGH concentrations.

A variety of technologies can be used to indirectly detect the presence of gas and fluid emissions from the seafloor. These include hydrographic surveys for particle rich or dissolved methane-rich thermal plumes (German et al., 2010; Baker and German, 2004), heat flow measurements (e.g. Lister, 1980; Fisher and Becker, 1991) and high-resolution seafloor imaging (e.g. De Beukelaer et al., 2003; Sahling et al., 2008; Klaucke et al., 2008). Both focused and diffuse gas and fluid emissions can be identified.

Water depths in the study area are deep enough for NGH to be stable. Combined with the availability of hydrate-forming gases, NGH can be anticipated within the GHSZ locally, although large concentrations will depend on the existence of fortuitously located sands. We have not identified NGH within the sediments in the area. We report the first use of high-resolution multibeam echo sounder data that includes water column data to identify subsea gas emissions in the offshore Barbados region.

2. Study area and background

The study area is located ~100 km southeast of Barbados along the Barbados Ridge, part of the Barbados Accretionary Complex (BAC) (Fig. 1). This region forms the eastern margin of the Caribbean Plate where the South and North American plates are being subducted beneath the BAC (Burke, 1988). Approximately 20 km of east–west shortened Quaternary – Miocene sediments, that are largely detached from the down-going slab, overly the detachment (Moore and Shipley, 1988). The sediments thicken toward the south as a consequence of increasing sediment burden and accretionary material flux originating from the ancestral and present-day Orinoco delta and its distal deep sea fan complexes (Westbrook et al., 1984). Two main bottom currents exist that help to shape the sediment bodies on the continental rise (Embley and Langseth, 1977): the North Atlantic Deep Water, that flows toward the southeast; and the Antarctic Bottom Water, that flows toward the northwest (Fig. 1). On the seafloor of the Barbados Ridge, the structural grain is dominantly north–south and mud volcanoes with diameters ranging up to ~8 km and craters are common (Fig. 1). Mud volcanoes, craters and faults have been mapped across the accretionary prism (Fig. 1) and natural gas emissions from the seafloor are spatially associated with mud diapirs (Brown and Westbrook, 1988; Körber et al., 2014) but previously, active gas emissions into the water column have neither been identified in this region nor associated with vent locations.

The composition of gases released from the emissions sites has not been measured *in-situ* in the study area. Geochemical inversion of hydrocarbon gases and liquids found in boreholes and natural seeps on Barbados indicates they are of a thermogenic origin and derived from marine Cretaceous source rocks (Hill and Schenk, 2005). On Trinidad and its surrounding offshore areas the gases are predominantly thermogenic mixed with a biogenic fraction (Battani et al., 2010; Deville et al., 2003a; Pohlman et al., 2009). Accordingly, the source of gas released from the seafloor is likely to be organic-rich shales that are part of the BAC, coupled with biogenic gas produced in the shallower subsurface.

NGH has been interpreted to be common in the study area. BSR, was used to indicate the presence of NGH (Brown and Westbrook, 1988; Deville et al., 2006, 2010; Marcelle-De Silva et al., 2012; Martin et al., 1996), but since the drilling on the Blake Ridge proved NGH with no underlying BSR and BSR with no overlying NGH (Holbrook, 2001), it is better understood that the negative impedance marker of the BSR is dominated by the presence of low Vp gas-enriched sediments, as has been shown by acoustic modeling (Max, 1990). NGH was recovered at a depth of 1 m in core KS20 collected ~200 km north of the study area (Martin et al., 1996).

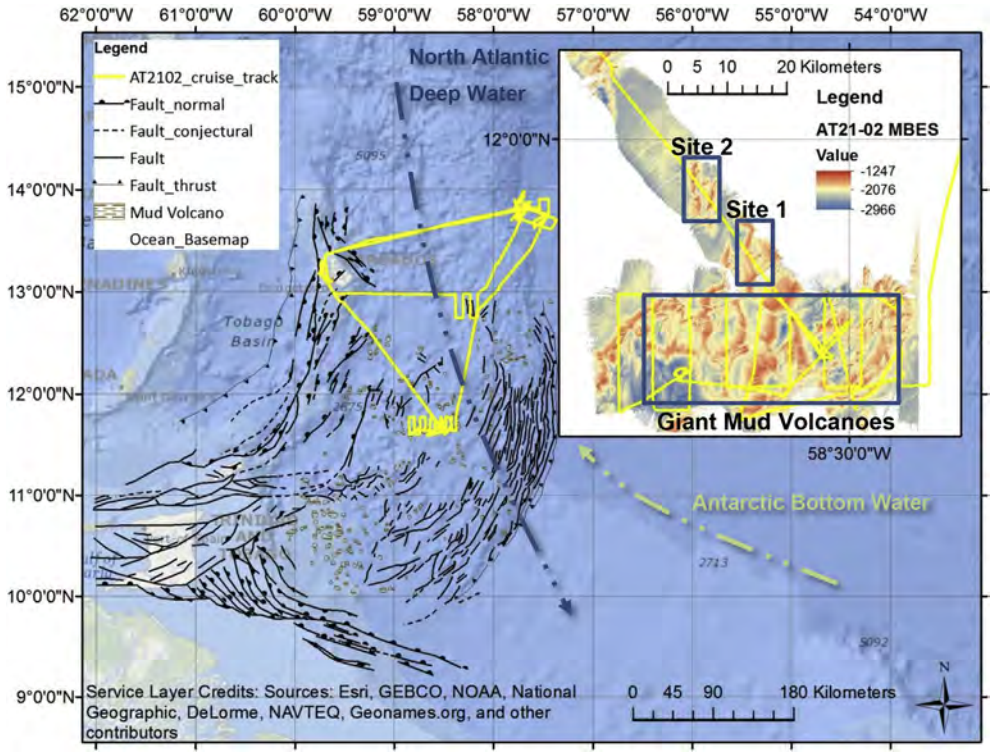

Figure 1. Locations of Site 1 and 2 along a northwest – southeast transect of the cruise track of the AT21-02 cruise from Barbados to several mud volcano sites within the Caribbean (yellow). Base map: structure of the southern Barbados Accretionary Complex and mud volcanoes (Deville et al., 2003b). The location and direction of deep water currents are provided for reference, and are adapted from Pichot et al. (2012). Inset: multibeam echo soundings (MBES) collected during cruise AT21-02 including the two sites discussed in detail in this paper. To the south of sites 1 and 2 is a region of giant ~8 km mud volcanoes. (For interpretation of the references to color in this figure legend, the reader is referred to the web version of this article.)

3. Multibeam echo soundings acquisition and processing methods – Atlantis AT21-02

Multibeam echo sounder data were collected as part of the underway geophysical data on the cruise Atlantis AT21-02 (Fig. 1). A Kongsberg-Simrad EM122 multibeam sonar system was used for mapping. This system has a dominant frequency of 12 kHz, 288 beams per ping and twin beams per ping when in multiping mode, which results in a greater sounding density and thus a higher data collection rate than in single ping mode (e.g., Sager et al., 2004a). The beam fan extends laterally 77° from vertical on both sides of the vessel and the beam spacing is related to water depth because of beam spread. Patch test (offsets and roll pitch, yaw corrections), sound velocity profiles and tidal information were applied to the

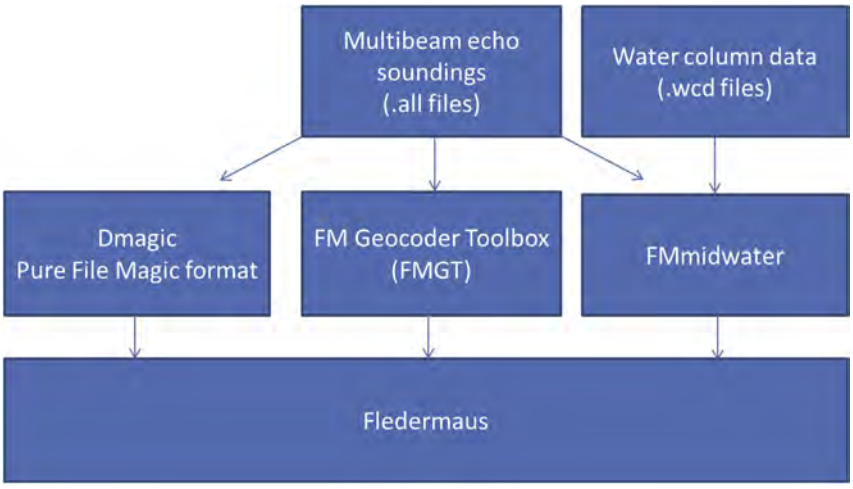

Figure 2. QPS multibeam processing workflow including the modules used. The Dmagic module processes multibeam data into multi-resolution bathymetric surfaces, FM Geocoder Toolbox creates qualitative and quantitative acoustic backscatter mosaics, FMmidwater allows the visualization and analysis of water column data, and the Fledermaus module integrates data from all the modules and allows visualization.

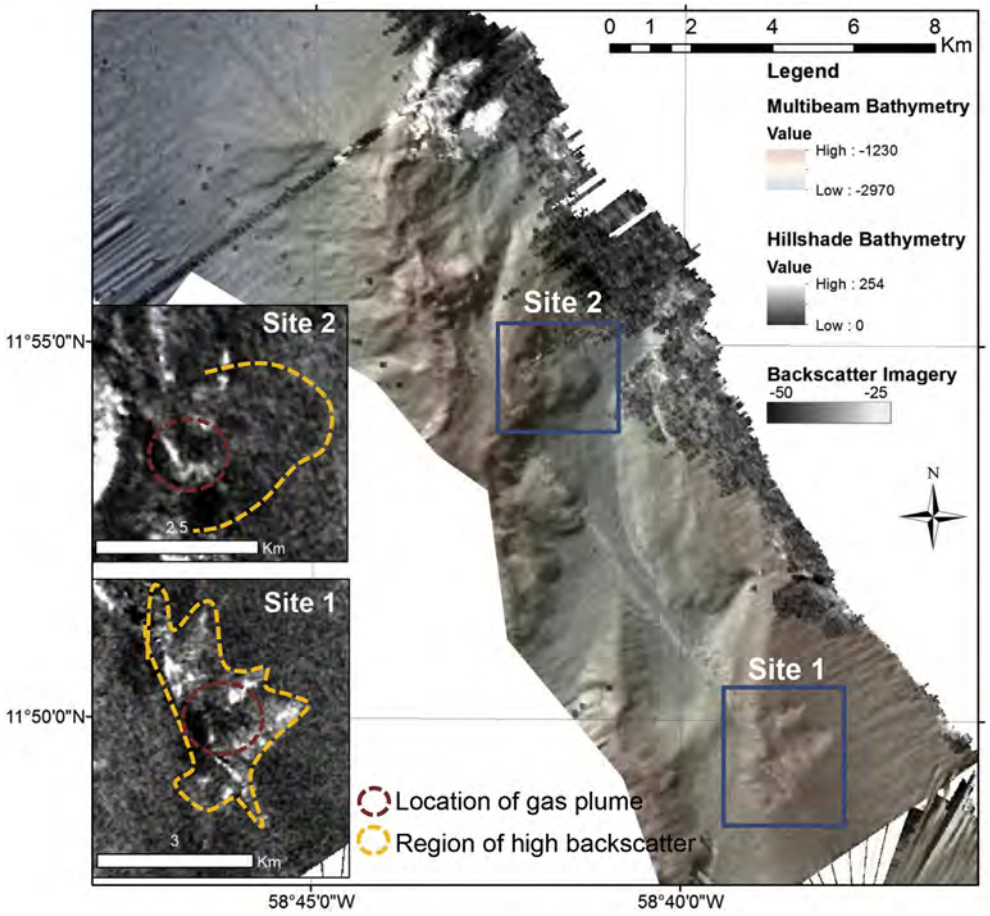

Figure 3. Base map: Sites 1 and 2 imaged by draping transparent multibeam bathymetry and hillshade layers over backscatter imagery. Illumination is cast from 315° at an altitude of 30°. Insets: regions of relatively high backscatter that cover the seafloor at sites 1 and 2.

swath sectors onboard. Raw multibeam data from the cruise AT21-02 are available from NOAA (http://www.ngdc.noaa.gov/mgg/bathymetry/multibeam.html). A northwest–southeast trending cruise line is used in this work that includes data not being studied by other groups.

The multibeam data were imported into the Quality Positioning Systems (QPS) software modules for processing, analysis and visualization (Fig. 2). Using the QPS modules allows the operator to process the bathymetry, backscatter, and water column data, fuse it together and analyze it in 4D (Doucet et al., 2009; Gee et al., 2012). The time dimension effectively provides the user with visualization of the data as it was collected using the acquisition time stamps, and also allows comparison of multiple passes or surveys. Based on the sounding density a 50 × 50 m cell size was chosen to create a map of seafloor bathymetry.

The fate of bubbles within gas plumes in the water column was investigated using the Colorado School of Mines CSMHYD software (Sloan and Koh, 2008). It was assumed that the top of the bubble plume marked the approximate upper limit of NGH stability as the disappearance of the high reflectance indicates transition to a gas–water contact rather than a NGH–water contact. Two modeled bubble gas compositions (87 and 100% methane) were entered into the program along with composite temperature data in order to determine the depth range of the water column GHSZ at different gas compositions. In the 87% methane model the remaining gas is composed of: ethane (7.6%), propane (3.1%), and small (<0.5%) amounts of i-butane, n-butane, nitrogen, n-pentane and isopentane. The composite temperature profile used in the model was created using a linear interpolation of temperature measurements (0–1500 m) from the AT21-02 survey data and Reid and Mantyla (1994).

4. Results

Extraction of the flares from the background water column data identifies the curvilinear shape of the anomalies and the extent of their resolvable travel time through the water column. Two sites have been identified along the cruise transect with water column anomalies that occur along narrow (~2 km), 7–10 km long, north–south trending ridges and valleys with ~400 m of relief (Fig. 3, Table 1). Flares within the water column occur at two sites at water depths between ~1500 and ~600 m depth (Figs. 4 & 5). At Site 1 two closely-spaced flares are both ~900 m tall whereas at site 2 the flares are shorter, ~600 m tall. Each has the higher amplitude backscatter values occurring in the central and lower portions of the flare, perhaps because this is the region of greatest bubble density (Kannberg et al., 2013), or an increase in reflectivity as the resonant frequency of single bubbles may be reached during their ascent (Lee et al., 2001).

Both sites occur on ridges adjacent to valleys. The steepest ridge slopes are ~20° and the ridge slope morphology has measured displacement/length ratios between 4 and 7, commonly associated with elliptical escarpments interpreted to mark the presence of faults and relays (Dawers and Anders, 1995; Walsh et al., 2002).

Table 1
Location of the identified seep sites (WGS84).

Site no.	Feature	Longitude	Latitude	Water depth (m)	Flare height (m)
1	Flares above craters	−58.6407	11.8273	~1470	~900
2	Flares above craters	−58.6985	11.9072	~1550	~600

Both sites display flares in the water column directly above hummocky seafloor with relatively high backscatter values. Large escarpments have been associated with mud volcanoes in the BAC region (northern Guiana Basin) by Langseth et al. (1988), who suggested that faults focus flow into migration pathways for ascending gas and fluids. The presence of flares in proximity with long linear ridges implies that these seafloor features are part of a deep plumbing system related to subjacent high pore fluid pressure, where the ridges are the surface termination of the faulting (e.g., Brown and Westbrook, 1988; Talukder, 2012; Westbrook and Smith, 1983).

Bathymetric expressions of gas and fluid emissions are also present at these sites where flares are absent in the water column. These regions are interpreted as the result of gas emissions that caused sediment redistribution including mud volcanism, which is typically associated with gas plumes emitted from the seafloor (e.g., Sager et al., 2003, 2004b). Multiple craters observed at site 1 may be satellite craters that formed on the flanks of a feeder channel (Tinivella and Giustiniani, 2012). At site 2, both craters and mud volcanoes occur beneath flares in the water column (Figs. 3 & 6). The absence of the gas plumes above some craters can be explained by the site being inactive, at least during the survey, because emissions were not occurring during data acquisition. Alternatively, emission rates at the time of survey could have been below the

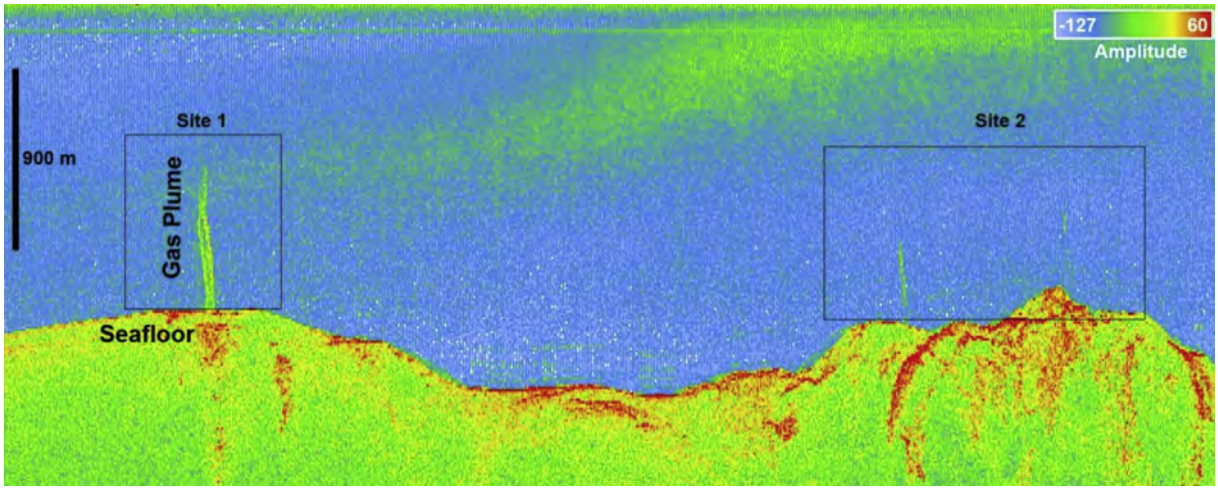

Figure 4. Along track water column data (view is perpendicular to the cruise track). Two regions where acoustic flares occur in the water column, sites 1 and 2. The flares are interpreted as gas plumes that ascend up to ~900 m through the water column. In this transect a maximum (dilation) filter is used to return the highest values for a neighborhood surrounding a pixel to identify targets in the water column (Doucet et al., 2009). In this image all of the data in the beam fan is visualized, all of the along track data is stacked to create this image. This image includes some distortion because it is not corrected for the beam angle in order to incorporate all of the information for all the beams. The amplitude values are the raw time series sample value present in the source sonar file, anomaly amplitudes are higher than the background water column values (Fig. 5).

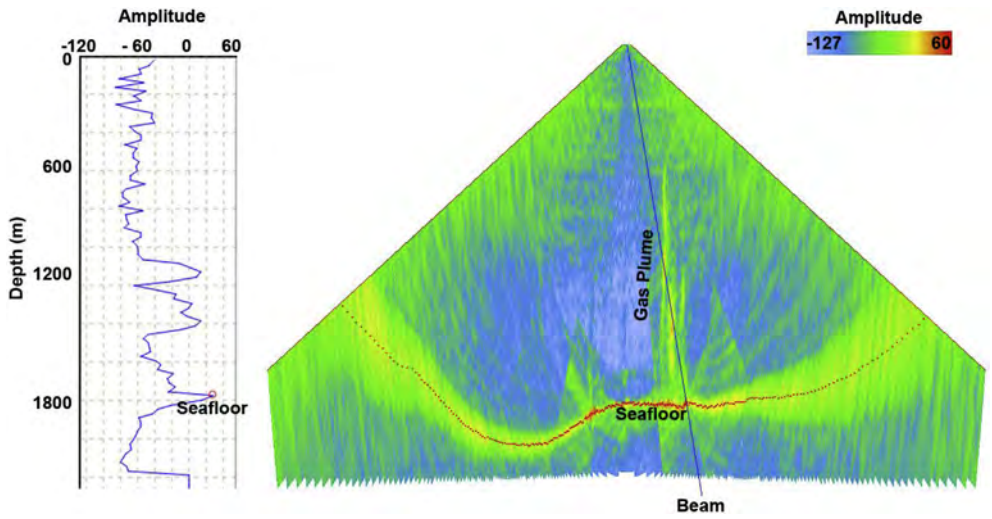

Figure 5. Site 1 beam fan with time series amplitude versus range (m) for a nearly vertical beam (~20° off nadir). Note that the flare is characterized by positive amplitudes higher than background water column values. The location of Site 1 is given in Figures 1 and 2, for color map see Figure 4. (For interpretation of the references to colour in this figure legend, the reader is referred to the web version of this article.)

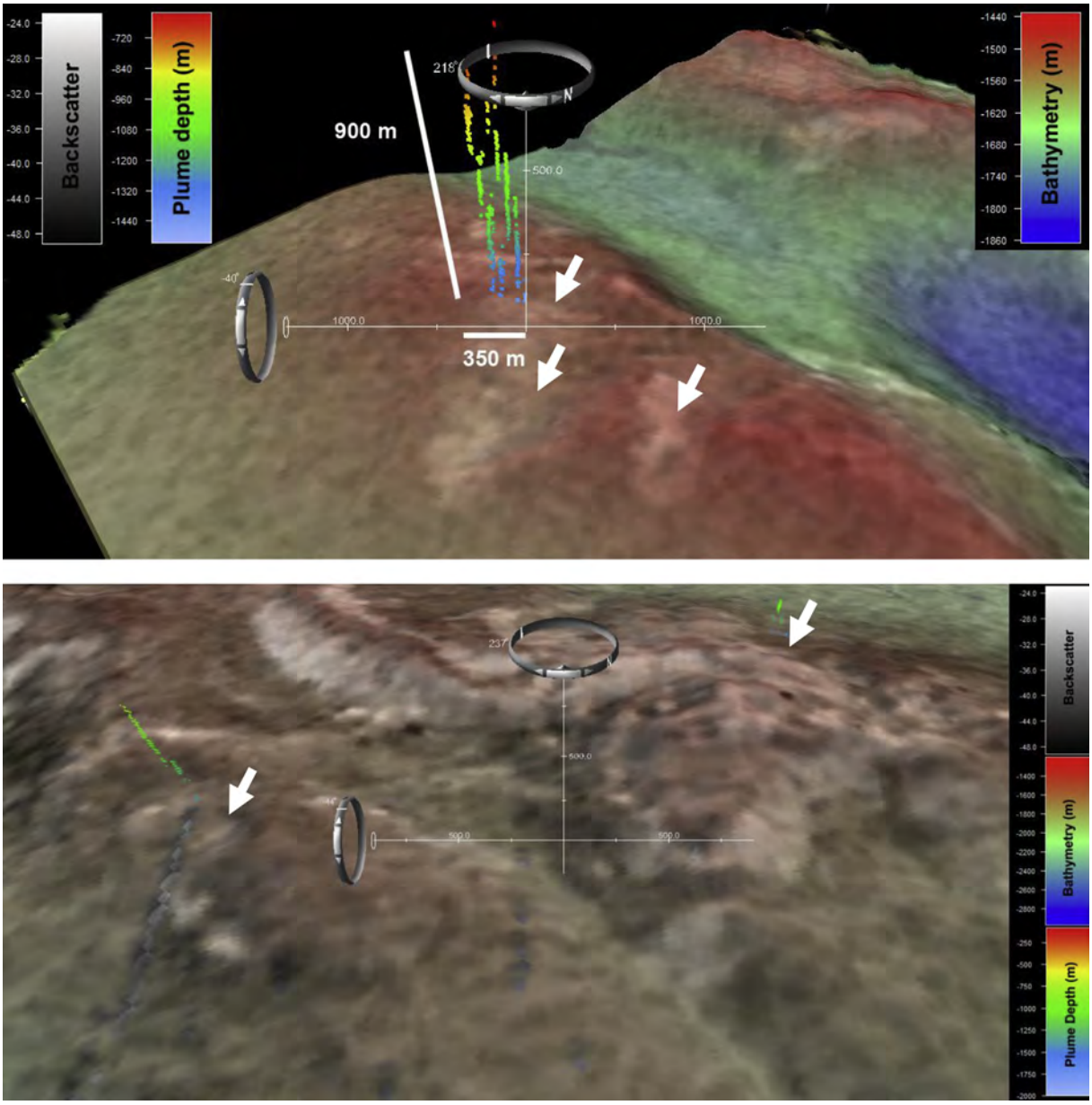

Figure 6. Integrated Fledermaus scene containing multibeam-bathymetry-shaded backscatter data with extracted water column data visualized as points. The upper panel is Site 1 and the lower is Site 2. Both sites occur along north–south trending long-linear ridges indicating that the plumes are associated with a deep plumbing system. White arrows mark cratered regions with high backscatter. Upper: site 1, multiple concentric high backscatter cratered regions are imaged beneath the plumes. The shear on the plume shows that the current direction is towards 128° (from the NW), and this view is orthogonal at 218° resulting in a view of the maximum shear from the water column with a shear angle of ~21° (white line). The flare is ~900 m tall, and is ~350 m offset from bottom to its top. The highest elevation in the foreground is −1470 m. Lower: site 2, gas plumes occur above cratered regions of high backscatter.

acoustic detection limits and rapidly dissolved. Sites with no water column anomalies are likely to be at least temporarily inactive, although the recurrence interval of the emissions is not known. It is unlikely that gas emissions below the acoustic detection limits could produce the observed seafloor craters and mud volcanism.

5. Discussion

5.1. Seafloor morphology associated with emissions sites

Large flares in the AT21-02 survey have been clearly identified at two sites. The flares are characterized by curvilinear shapes that cross sonar transmit sectors and rise 600–900 m through the water column. The flares are distinct features that do not have the characteristics of data artifacts that can be caused by the interaction of sound in water and which are characterized as 'smiles', 'frowns,' and linear features depending on their cross-section appearance (Marques and Clarke, 2012). Side lobe and previous ping interference also cause false bottom echoes (Cobra, 1990; Tomczak et al., 2002). However, the flares in the AT21-02 data are clearly resolved in acoustic images and are interpreted as plumes of gas rising from the seafloor.

On the seafloor beneath the gas plumes circular regions of hummocky or complex morphology with high backscatter are common (Fig. 6). In addition, changes in sediment properties that cause acoustic backscatter anomalies in the ensonified region also

occur (Blondel and Murton, 1997). The annular, higher amplitude backscatter regions beneath the gas plumes are interpreted as sediment brought to the seafloor as a result of mud volcanism. Dewatering has produced relatively compacted sediment that has higher backscattered energy than adjacent sediment (Sager et al., 2003, 2004b). Additionally, the observation of multiple concentric higher scattering regions implies that the emissions have either: 1) moved location locally or, 2) been present at multiple sites having varying gas/water flow rate or volume. Temporal changes in the emissions discharged and pathways used could be related to restriction of permeability caused by NGH within the gas and fluid pathways. Because of the similar sizes of each eruption site identified, the volumes of fluid and gas do not appear to have been significantly different from place to place. The maximum emissions at each location are similar indicating that there is some sort of damping function on sediment distribution caused by the seawater. The emission sites have only local satellite craters, which suggests that the deep plumbing system feeding the gas plumes has not moved laterally by a large distance and has a focused flow migration path.

Migration routes that lead to natural hydrocarbon seeps at the seafloor can be used to establish the presence of an effective and generating petroleum system at depth (McConnell et al., 2008). Determining whether a region is a gas province with a strong gas flux is one of the first steps in hydrate petroleum system exploration (Max and Johnson, 2014). In the study area north–south trending faults are associated with seafloor gas emissions (e.g., Plaza-Faverola et al., 2015). As well as pointing to petroleum systems it is possible that migratory gas flow can be so large that few hydrocarbons remain in the sediments as they escape entrapment (Løseth et al., 2009, 2011). Although gas flows can be large, unless the other requirements for forming NGH concentrations exist, there may be little NGH sequestration of natural gas.

5.2. Ascending gas bubbles

Formation of NGH shells on bubbles is well understood (Max, 2003; Max et al., 2006, and references therein) and have been observed in both the laboratory and field (Maini and Bishnoi, 1981; Rehder et al., 2002). Data from artificially simulated bubble releases within the GHSZ demonstrates that the formation of NGH shells inhibits mass transfer across the bubble wall, effectively armoring the bubble from dissolution (Rehder et al., 2002; Warzinski et al., 2014).

Based on the single bubble dissolution model presented by McGinnis et al. (2006) a 10 mm bubble with a NGH shell can ascend ~900 m through the water column whereas an unarmored bubble must be ~40 mm in diameter to make an ascent of a similar duration. Such large bubbles are predicted to be either unlikely or to break apart into smaller bubbles (McGinnis et al., 2006). Model runs using the single bubble dissolution model, SiBuGUI, (Greinert and McGinnis, 2009; McGinnis et al., 2006) highlight the influence the GHSZ has on bubble dissolution through its impact on the gas exchange coefficient. Ascending bubbles, upon crossing the GHSZ, rapidly decrease in size, a phenomenon related to a relative increase in the rate of dissolution following disappearance of their NGH shell.

5.3. Temperature and multibeam water column data

A model of the depth of the GHSZ using CSMHYD based on the phase requirements for NGH formation, temperature data and bubble compositions of 100% and 87% methane indicates that the top of the GHSZ boundary occurs at ~600 m and ~300 m, respectively (Fig. 7). Similarly, the tallest gas plume (Site 1) reaches from the seafloor up to ~600 m water depth. The observed top of the gas plume does not correspond exactly to the three horizontal hydrographic water masses in the water column that have been identified by correlating amplitude values in the multibeam water column data with temperature data from conductivity, temperature, depth casts. These layers are: 1) the shallow surface (mixed) layer above 100 m; 2) a middle layer ~100–250 m; and 3) a lower layer 250–2000 m. The surface mixed layer is positioned above ~100 m and the thermocline penetrates to ~250 m, both are significantly higher in the water column than the top of the acoustic flare (~600 m). Disappearance of the flare at ~600 m does not correspond to a water layer boundary, so the disappearance does not appear related to a rapid change in water properties, especially in temperature. In contrast, the acoustic signature of the plumes at Site 2 is much smaller and does not persist to such high levels in the water column. This is likely because the volumes of gas contained within the plumes are smaller, or the released bubble size is smaller, so the plume bubbles disappear at a greater depth.

The precise depth of bubble dissolution cannot explicitly be resolved solely from acoustic signal data, because the imaging of bubbles is controlled by acoustic resolution as well as bubble size and density. Although the abrupt disappearance of the acoustic signature of the vent gas/water at ~600 m may be a result of a significant change in bubble character, to disappearance of NGH shells, it is also possible that bubbles are present below the threshold size and density to cause an acoustic return. Consequently, water column images indicate the maximum depth of bubble dissolution. The simplest explanation is that bubbles disappear at ~600 m because they lose their NGH shell and are quickly dissolved thereafter.

5.4. Vent gas potential as an atmospheric greenhouse component

There has been little or no quantification of the amount of gas that reaches the atmosphere from subsea gas emissions. It's known that armored bubbles and storms can transfer gas from the seafloor to the atmosphere (Leifer et al., 2004; Brewer, 2014). Yet almost all of the estimates concern the amount of gas, particularly methane, released from the seafloor.

Gases that may reach the atmosphere from anthropogenic sources, such as the Macondo well in the northern Gulf of Mexico, are special cases (e.g., Hopkins, 2012). In multiphase vent flow, gas may ascend dissolved in the oil, or as part of a violently ascending fluidized mixture of water, and gas. Naturally produced hydrocarbons venting from the seafloor sustain communities of hydrocarbon-degrading bacteria that scale their populations to the volumes of hydrocarbons available (Smith et al., 2014). Kessler et al. (2011) and Joye et al. (2014) note that during the Macondo blowout much of the liquid petroleum and virtually all of the gaseous hydrocarbons remained in the deep ocean where microbiological degradation essentially and quickly respired the methane. Joye et al. (2011) refer to a high concentration of dissolved gas 1000–1300 m above the ~1520 m deep wellhead.

In the region of the AT21-02 survey, water depths of 1500 m are great enough and temperatures and salinity low enough for the local mixture of gases to be stable enough below ~600 m for NGH shells to form. Thus, because they are highly reflective, it is virtually certain that the bubbles imaged in this study are armored by NGH shells for the first part of their ascent to the surface. Most gas emissions that have been mapped in this survey and other scientific study areas appear to be relatively clean and free of petroleum contamination. Thus, the physical chemistry and diffusional mechanisms that control NGH growth, dissociation, and dissolution should be relatively predictable.

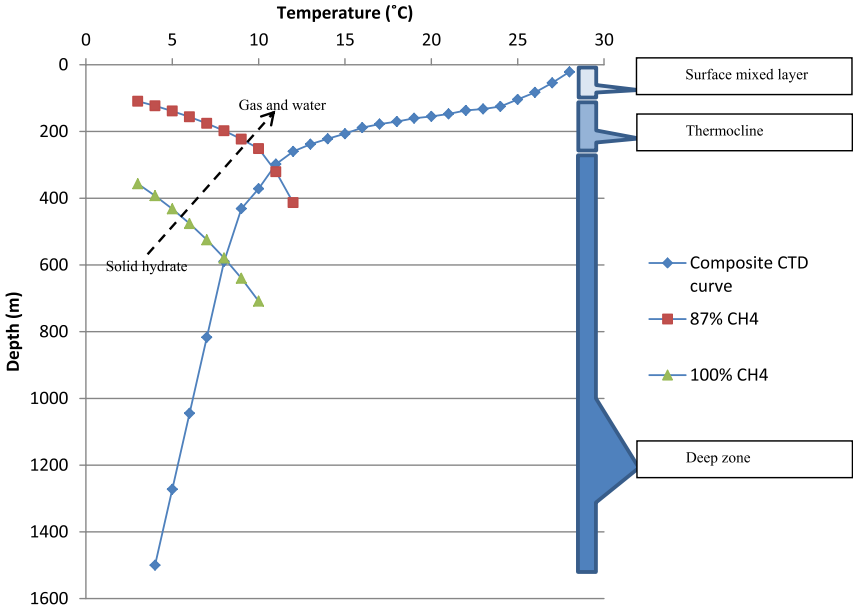

Figure 7. The composite CTD curve is an approximation of the water column temperature in the study region and is presented with an interpretation of the stratification of the surface to deep layers. The composite CTD curve is based on a representative CTD cast from AT21-02 cruise from 0 to 400 m and an equal interval linear interpolation to seafloor data from the Reid and Mantyla (1994) dataset, courtesy of GeoMapApp (http://www.geomapapp.org). The modeled gas hydrate stability zone was created using CSMHYD (http://hydrates.mines.edu/CHR/Software.html). The 87 and 100% methane gas hydrate stability zone models cross the CTD curve at 300 and 600 m, respectively and are used to estimate the depth of gas hydrate dissociation in the water column.

Although NGH is mechanically strong (Durham et al., 2003), during ascent the shells lie in a tensional strain field, in which materials are at their weakest. As the gas bubbles ascend, the pressure between the interior gas and the surrounding pressure field increases as depth shallows. The dominant control to bubble integrity is pressure change in the pressure differential between the trapped gas and the exterior seawater source (Leifer et al., 2004).

Initially upon venting from the subsurface into the seawater, gas bubbles resolve into the most stable physical size for the pressure depth and gas composition (Fig. 8, A). As the NGH-armored bubbles rise, they reach a point where the pressure differential on the shell causes them to begin to start breaking (Fig. 8, B). Between A and B, acoustic reflection is mainly from bubble surfaces. Above that the rate of change of pressure differential increases according to Boyle's Law and further bubble shell rupture and formation can be anticipated perhaps multiple times. Therefore, as the bubble mass rises, the ratio of gas to NGH decreases and with each rupture and reshell, the surface area of NGH to mass increases (Fig. 8, C). This is important for the rate of dissociation above the depth of NGH stability (Fig. 8, D) because dissociation is a diffusion controlled surface effect at NGH–water boundaries (Max et al., 2006). In addition, as NGH replaces gas, the overall buoyancy will decrease, allowing more time for conversion to NGH and for dissolution.

Prior to the bubbles with NGH shells exiting from their field of stability, and when a large part of the original gas is either contained within NGH-shelled bubbles or is within NGH and if the concentration of dissolved gas molecules in the bounding seawater is low enough (Fig. 8, zone C–D), the outer part of the NGH shell will begin to dissolve directly into the seawater, even as bubbles shatter and more of the gas within bubbles forms new NGH. The resulting fluidized mass of ascending gas and NGH result in a highly reflective cloud of smaller gas bubbles shell shards, which have the potential to reflect acoustic energy in much the same manner that chaff used to foil radar does.

As soon as ascending gas bubbles with NGH shells pass through the upper limit of NGH stability that extends to the surface (Fig. 8, E), wholesale dissociation begins with an increased availability of gas molecules at shell or shard-water wall contacts. Because molecular methane is being produced at the boundary, very rapid direct dissolution is likely, especially if there is substantial turbulence and mixing that brings undersaturated seawater in contact with the NGH shells.

Because much of the original vent gas has been converted to NGH, whose dissociation facilitates dissolution, greater volumes of gas can be expected to be dissolved into the seawater. The NGH shards ascend more slowly than gas, which allows more time for dissociation and dissolution, the nearer surface waters tend to have faster currents and higher turbulence, which accelerates dissolution, and unshelled gas bubbles are smaller, with higher surface area to mass ratios, which also facilitate rapid dissolution. Thus, assuming that much of the gas simply rises through the seawater and reaches the atmosphere may strongly overstate the amount of vent gas that may not be dissolved in the seawater.

There is a need for detailed emission site inventories and ways to quantify emissions with integrated seafloor and water column datasets. In particular, measurement of gas vent parameters, NGH conversion and dissolution characteristics from a vent to the surface is necessary before assuming that any volume of vent gas reaches the atmosphere where it could contribute to the thermal greenhouse.

5.5. Current velocity analysis

As bubbles rise they will tend to behave as Lagrangian drifters, making them useful as ocean current indicators. Using the threshold technique of Doucet et al. (2009), it is possible to visualize the shear imparted by current on bubble plumes at depth (Fig. 6 Upper). Consequently, the direction of the current and a qualitative sense of velocity can be determined by the maximum shear angle of a plume of gas bubbles in the water column. In this area the current flowed from the northwest towards the southeast at ~128° during the time of the survey. The gas plumes rise ~900 m and the horizontal difference between the top and the base is a

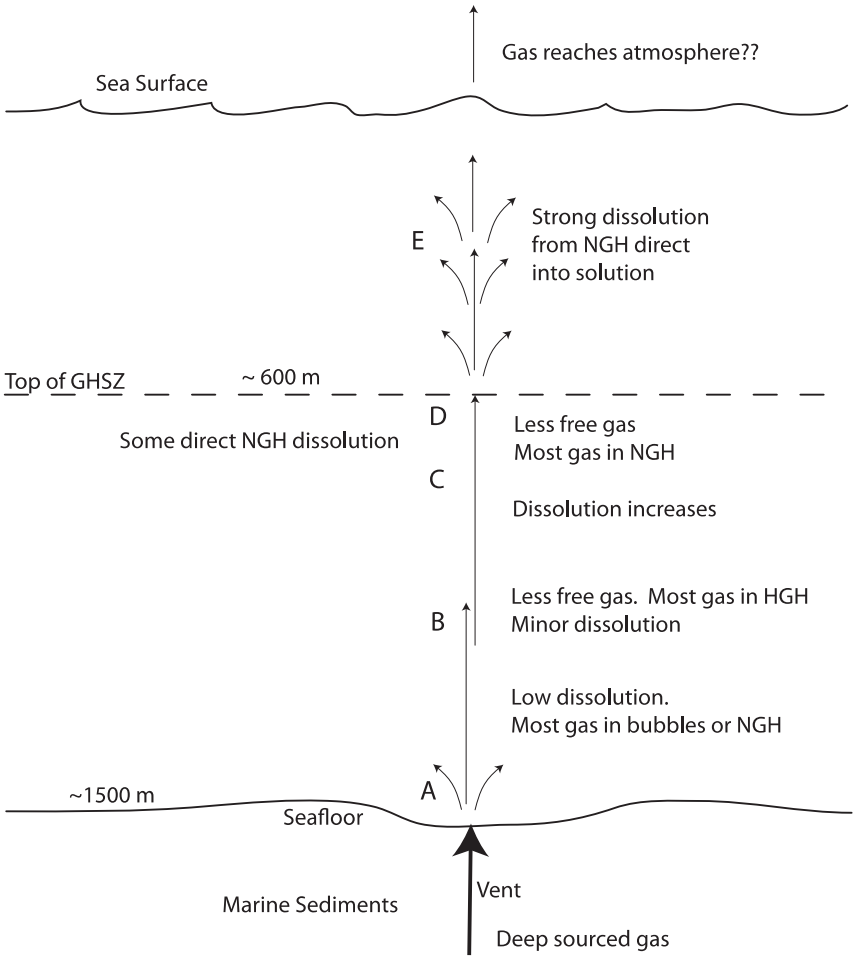

Figure 8. Schematic representation of ascending gas/NGH from vent toward sea surface.

maximum of ~350 m at 128° azimuth, yielding an average ~21° of flare tilt off vertical. Using an average ascent rate of 20 cm/s for bubbles 1–10 mm in diameter implies a current velocity of 8–10 cm/s, similar to the value of 10 cm/s measured in this region by Crease (1962).

The tilt of the plume reflects the current direction above the emission site but from the available data it is not possible to determine velocity or whether the current is a local or regional feature. Deep water currents can also be related to small-scale abyssal undular vortices (Rubino et al., 2012). Our results cannot rule out the presence of abyssal vortices, which could complicate the interpretation of the current direction. The possibility exists that the observed current direction is not representative of average mean transport, although the estimated current direction is consistent with measured velocities (Crease, 1962) and is in agreement with the southeasterly current direction of North Atlantic Deep Water that flows over the BAC (Pichot et al., 2012). Because the Antarctic Bottom Water and North Atlantic Deep Water are different temperatures, temporal variations in these deep currents are important because focused gas emissions in shallow gas NGH systems have been shown to be sensitive to bottom water temperatures (Berndt et al., 2014).

6. Conclusions

Two subsea sites with gas plumes 600-900 m high in the water column have been identified using water column multibeam data in the sea area of the Barbados Accretionary Complex. The gas plumes are in close proximity with north–south trending faults and appear to be associated with a deeper plumbing system. Association of the gas plumes with seafloor mud volcanoes is evidence for gas-driven venting and mud volcanism.

The calculated horizontal shear of the gas plumes is consistent with a current direction and velocity similar to that of North Atlantic Deep Water in this region. Bubble ascent ~900 m through the water column is made possible through the formation of NGH shells on gas bubble walls. Disappearance of the gas plumes at ~600 m depth is likely related to the dissolution of the NGH gas shell armoring and shards at the top of the GHSZ within the water column. Although it is not possible to quantify methane volume flux based on the available data the widespread occurrence of mud volcanoes across the Barbados Accretionary Complex suggest that it is substantial (e.g., Murton and Biggs, 2003).

Direct acoustic studies of subsea gas emissions are now capable of enabling quantitative estimates of gas volume (Weber et al., 2014). The volumes and rate of temporal change are important elements for understanding natural fluxes of hydrocarbons entering the oceans and their potential to reach the atmosphere (e.g., Solomon et al., 2009) but acoustic observations of smaller gas-based sites suggest that the gases dissolve in the sea and do not reach the atmosphere (McGinnis et al., 2006; Weber et al., 2014). Characterization of regions of the seafloor where emissions occur, better estimates of the gases released into the ocean, and further documentation of the processes involved and quantities of gas that

reach the atmosphere are needed to not only isolate anthropogenic gas sources but also to further understand how subsea gas emissions impact climate and global change.

All methane emitting from land sources enters the atmospheric biosphere. From 2003 to 2009, the Four Corners area released a little over 4 million metric tons of methane into the atmosphere and the map of US methane emissions shows very few areas (pixels) that do not vent methane directly from the land to the atmosphere (Kort et al., 2014). These new estimates are about 3.5 times the estimate for the same area in the current Emissions Database for Global Atmospheric Research. This implies that global methane emission from land areas to the atmosphere may be larger than previously estimated. In contrast, not only are there very imperfect estimates for methane venting into the ocean, the estimates for what percentage of marine methane could reach the atmosphere are even more imperfectly understood.

Acknowledgments

Thanks to the crew and scientists of the R/V Atlantis during AT21-02, particularly Cindy Van Dover. Thanks to Bill Chadwick, Susan Merle, Daniel Price and Evan Robertson from NOAA, Erin Heffron, Lindsay Gee and the staff at QPS, Bramley Murton (NOCS). A special thank you to Dan McGinnis for providing us with a copy of the single bubble dissolution model SibuGUI. Thanks to Jingqiu Huang for discussion of acoustic imaging and Julia Wellner for organizing a full semester of gas-hydrate related talks at UH. We would also like to thank John Casey and an anonymous reviewer for their support and constructive comments that significantly improved this paper. This research was funded by the University of Houston, Department of Earth and Atmospheric Sciences Teaching Assistantship.

References

Agirrezabala, L.M., Kiel, S., Blumenberg, M., Schäfer, N., Reitner, J., 2012. Outcrop analogues of pockmarks and associated methane-seep carbonates: a case study from the Lower Cretaceous (Albian) of the Basque-Cantabrian Basin, western Pyrenees. Palaeogeogr. Palaeoclimatol. Palaeoecol. 390, 94–115.

Aloisi, G., Pierre, C., Rouchy, J.-M., Foucher, J.-P., Woodside, J., 2000. Methane-related authigenic carbonates of eastern Mediterranean Sea mud volcanoes and their possible relation to gas hydrate destabilisation. Earth Planet. Sci. Lett. 184, 321–338.

Baker, E.T., German, C.R., 2004. On the global distribution of mid-ocean ridge hydrothermal vent fields. In: German, C.R., Lin, J., Parson, L.M. (Eds.), Mid-ocean Ridges: Hydrothermal Interactions Between the Lithosphere and Oceans. AGU, Washington, DC, pp. 245–266.

Bayrakci, G., Scalabrin, C., Dupré, S., Leblond, I., Tary, J.B., Lanteri, N., Augustin, J.M., Berger, L., Cros, E., Ogor, A., Tsabaris, C., Lescanne, M., Géli, L., 2014. Acoustic monitoring of gas emissions from the seafloor. Part II: a case study from the Sea of Marmara. Mar. Geophys. Res. 35 (3), 211–229.

Battani, A., Prinzhofer, A., Deville, E., Ballentine, C.J., 2010. Trinidad mud volcanoes: the origin of the gas. In: Wood, L. (Ed.), Shale Tectonics, AAPG Memoir 93, pp. 225–238.

Berndt, C., Feseker, T., Treude, T., Krastel, S., Liebetrau, V., Niemann, H., Bertics, V.J., Dumke, I., Dünnbier, K., Ferré, B., Graves, C., Gross, F., Hissmann, K., Hühnerbach, V., Krause, S., Lieser, K., Schauer, J., Steinle, L., 2014. Temporal constraints on hydrate-controlled methane seepage off Svalbard. Science 343 (6168), 284–287.

Bian, Y., Feng, D., Roberts, H.H., Chen, D., 2013. Tracing the evolution of seep fluids from authigenic carbonates: Green Canyon, northern Gulf of Mexico. Mar. Pet. Geol. 44, 71–81.

Blackford, J., Stahl, H., Bull, J.M., Berges, B.J.P., Cevatoglu, M., Lichtschlag, A., Connelly, D., James, R.H., Kita, J., Long, D., Naylor, M., Shitashima, K., Smith, D., Taylor, P., Wright, I., Akhurst, M., Chen, B., Gernon, T.M., Hauton, C., Hayashi, M., Kaieda, H., Leighton, T.G., Sato, T., Sayer, M.D.J., Suzumura, M., Tait, K., Vardy, M.E., White, P.R., Widdicombe, S., 2014. Detection and impacts of leakage from sub-seafloor deep geological carbon dioxide storage. Nat. Clim. Change 4, 1011–1016.

Blondel, P., Murton, B.J., 1997. Handbook of Seafloor Sonar Imagery. Wiley, UK.

Brewer, P., 2014. Marine biogeochemistry: Arctic shelf methane sounds alarm. Nat. Geosci. 7 (1), 6–7.

Bohrmann, G., Greinert, J., Suess, E., Torres, M., 1998. Authigenic carbonates from the Cascadia subduction zone and their relation to gas hydrate stability. Geology 26, 647–650.

Boles, J., Clark, J., Leifer, I., Washburn, L., 2001. Temporal variation in natural methane seep rate due to tides, Coal Oil Point area, California. J. Geophys. Res. Oceans (1978–2012) 106, 27077–27086.

Bonini, M., 2012. Mud volcanoes: indicators of stress orientation and tectonic controls. Earth Sci. Rev. 115 (3), 121–153.

Brothers, L.L., Kelley, J.T., Belknap, D.F., Barnhardt, W.A., Andrews, B.D., Legere, C., Hughes Clarke, J.E., 2012. Shallow stratigraphic control on pockmark distribution in north temperate estuaries. Mar. Geol. 329, 34–45.

Brown, K., Westbrook, G.K., 1988. Mud diapirism and subcretion in the Barbados Ridge Accretionary Complex: the role of fluids in accretionary processes. Tectonics 7, 613–640.

Burke, K., 1988. Tectonic evolution of the Caribbean. Annual Review of Earth and Planetary Sciences 16, 201–230.

Cao, Y., Su, Z., Chen, D., 2013. Influence of water flow on gas hydrate accumulation at cold vents. Sci. China Earth Sci. 56 (4), 568–578.

Chand, S., Rise, L., Ottesen, D., Dolan, M., Bellec, V., Bøe, R., 2009. Pockmark-like depressions near the Goliat hydrocarbon field, Barents Sea: morphology and genesis. Mar. Pet. Geol. 26, 1035–1042.

Cobra, D.E.Q., 1990. Estimation and Correction of Geometric Distortions in Side-scan Sonar Images (Unpublished doctoral dissertation). Massachusetts Institute of Technology/Woods Hole Oceanographic Institution, USA.

Colbo, K., Ross, T., Brown, C., Weber, T., 2014. A review of oceanographic applications of water column data from multibeam echosounders. Estuar. Coast. Shelf Sci. 145, 41–56.

Crease, J., 1962. Velocity measurements in the deep water of the western North Atlantic: summary. J. Geophys. Res. 67, 3173–3176.

Daigle, H., Bangs, N.L., Dugan, B., 2011. Transient hydraulic fracturing and gas release in methane hydrate settings: a case study from southern Hydrate Ridge. Geochem. Geophys. Geosyst. 12, Q12022.

Dawers, N.H., Anders, M.H., 1995. Displacement-length scaling and fault linkage. J. Struct. Geol. 17, 607–614.

Dawson, A., Bondevik, S., Teller, J., 2011. Relative timing of the Storegga submarine slide, methane release, and climate change during the 8.2 ka cold event. Holocene 21, 1167–1171.

De Beukelaer, S.M., MacDonald, I.R., Guinnasso, N.L., Murray, J.A., 2003. Distinct side-scan sonar, RADARSAT SAR, and acoustic profiler signatures of gas and oil seeps on the Gulf of Mexico slope. Geo-Mar. Lett. 23, 177–186.

Denman, K.L., Brasseur, G., Chidthaisong, A., Ciais, P., Cox, P.M., Dickinson, R.E., Hauglustaine, D., Heinze, C., Holland, E., Jacob, D., 2007. Couplings between changes in the climate system and biogeochemistry. Clim. Change 2007, 541–584.

Deville, É., Battani, A., Griboulard, R., Guerlais, S., Lallemant, S., Mascle, A., Prinzhofer, A., Schmitz, A., 2003a. Processes of Mud Volcanism in the Barbados-Trinidad Compressional System: New structural, Thermal and Geochemical Data. Geological Society, Search and Discovery Article, 30017(9).

Deville, É., Mascle, A., Guerlais, S.-H., Decalf, C., Colletta, B., 2003b. Lateral changes of frontal accretion and mud volcanism processes in the Barbados accretionary prism and some implications. AAPG Mem. 79, 656–674.

Deville, É., Guerlais, S.-H., Callec, Y., Griboulard, R., Huyghe, P., Lallemant, S., Mascle, A., Noble, M., Schmitz, J., 2006. Liquefied vs stratified sediment mobilization processes: insight from the South of the Barbados accretionary prism. Tectonophysics 428, 33–47.

Deville, É., Guerlais, S.-H., Lallemant, S., Schneider, F., 2010. Fluid dynamics and subsurface sediment mobilization processes: an overview from Southeast Caribbean. Basin Res. 22, 361–379.

Dillon, W.P., Nealon, J.W., Taylor, M.H., Lee, M.W., Drury, R.M., Anton, C.H., 2001. Seafloor collapse and methane venting associated with gas hydrate on the Blake Ridge - causes and implications to seafloor stability and methane release. In: Paull, C.K., Dillon, W.P. (Eds.), Natural Gas Hydrates Occurrence, Distribution and Detection, American Geophysical Union Geophysical Monograph 124, pp. 211–234.

Doucet, M., Ware, C., Arsenault, R., Weber, T., Malik, M.A., Mayer, L., Gee, L., 2009. Advanced mid-water tools for 4D marine data fusion and analysis. In: Proceedings of OCEANS 2009, MTS/IEEE Biloxi-Marine Technology for Our Future: Global and Local Challenges. IEEE, pp. 1–9.

Durham, W.B., Kirby, S.H., Stern, L.A., Zhang, Wu, 2003. The strength and rheology of methane clathrate hydrate. J. Geophys. Res. 108 (B4) http://dx.doi.org/10.1029/2002JB001872, 11 pp.

Embley, R.W., Langseth, M.G., 1977. Sedimentation processes on the continental rise of northeastern South America. Mar. Geol. 25, 279–297.

Fisher, A.T., Becker, K., 1991. Heat flow, hydrothermal circulation and basalt intrusions in the Guaymas Basin, Gulf of California. Earth Planet. Sci. Lett. 103, 84–99.

Fisher, R.E., Sriskantharajah, S., Lowry, D., Lanoisellé, M., Fowler, C., James, R., Hermansen, O., Lund Myhre, C., Stohl, A., Greinert, J., 2011. Arctic methane sources: isotopic evidence for atmospheric inputs. Geophys. Res. Lett. 38 (21), L21803.

Gee, L., Doucet, M., Parker, D., Weber, T., Beaudoin, J., 2012. Is multibeam water column data really worth the disk space?. In: Proceedings of Hydro12 – Taking Care of the Sea, San Diego, CA, pp. 81–86.

German, C.R., Bowen, A., Coleman, M.L., Honig, D.L., Juber, J.A., Jakuba, M., Kinsey, J.C., Kurz, M.D., Leroy, S., McDermott, J.M., Mercier de Lepinay, B.,

Nakamura, K., Seewald, J.S., Smith, J.L., Sylva, S.P., Van Dover, C.L., Whitcomb, L.L., Yoerger, D.R., 2010. Diverse styles of submarine venting on the ultraslow spreading Mid-Cayman Rise. Proc. Natl. Acad. Sci. 107 (32), 14020–14025.
Greinert, J., Artemov, Y., Egorov, V., De Batist, M., McGinnis, D., 2006. 1300-m-high rising bubbles from mud volcanoes at 2080m in the Black Sea: hydroacoustic characteristics and temporal variability. Earth Planet. Sci. Lett. 244, 1–15.
Greinert, J., 2008. Monitoring temporal variability of bubble release at seeps: the hydroacoustic swath system GasQuant. J. Geophys. Res. Oceans 113, C7.
Greinert, J., McGinnis, D.F., 2009. Single bubble dissolution model: the graphical user interface – SiBu-GUI. Environ. Model. Softw. 24, 1012–1013.
Haeckel, M., Suess, E., Wallmann, K., Rickert, D., 2004. Rising methane gas bubbles form massive hydrate layers at the seafloor. Geochim. Cosmochim. Acta 68, 4335–4345.
Hill, R.J., Schenk, C.J., 2005. Petroleum geochemistry of oil and gas from Barbados: implications for distribution of Cretaceous source rocks and regional petroleum prospectivity. Mar. Pet. Geol. 22, 917–943.
Holbrook, W.S., 2001. Seismic studies of the Blake Ridge: implications for hydrate distribution, methane expulsion and free gas dynamics. In: Paull, C.K., Dillon, W.P. (Eds.), Natural Gas Hydrates: Occurrence, Distribution and Detection. AGU, Washington, DC, pp. 235–256.
Hopkins, A., 2012. Disastrous Decisions: the Human and Organizational Causes of the Gulf of Mexico Blowout. CCH Australia Ltd.
Hovland, M., Jensen, S., Fichler, C., 2012. Methane and minor oil macro-seep systems — their complexity and environmental significance. Mar. Geol. 332, 163–173.
Hyndman, R., Spence, G., 1992. A seismic study of methane hydrate marine bottom simulating reflectors. J. Geophys. Res. Solid Earth (1978–2012) 97, 6683–6698.
Jerosch, K., Schlüter, M., Foucher, J.-P., Allais, A.-G., Klages, M., Edy, C., 2007. Spatial distribution of mud flows, chemoautotrophic communities, and biogeochemical habitats at Håkon Mosby Mud Volcano. Mar. Geol. 243, 1–17.
Johnson, J.E., Goldfinger, C., Suess, E., 2003. Geophysical constraints on the surface distribution of authigenic carbonates across the Hydrate Ridge region, Cascadia margin. Mar. Geol. 202, 79–120.
Jones, T.D., Ridgwell, A., Lunt, D., Maslin, M., Schmidt, D., Valdes, P., 2010. A Palaeogene perspective on climate sensitivity and methane hydrate instability. Philos. Trans. R. Soc. A Math. Phys. Eng. Sci. 368, 2395–2415.
Joye, S.B., MacDonald, I.R., Leifer, I., Asper, V., 2011. Magnitude and oxidation potential of hydrocarbon gases released from the BP oil well blowout. Nat. Geosci. 4, 160–164.
Joye, S.B., Teske, A.P., Kostka, J.E., 2014. Microbial dynamics following the Macondo oil well blowout across gulf of Mexico environments. BioScience 64 (9), 766–777.
Kannberg, P.K., Tréhu, A.M., Pierce, S.D., Paull, C.K., Caress, D.W., 2013. Temporal variation of methane flares in the ocean above Hydrate Ridge, Oregon. Earth Planet. Sci. Lett. 368, 33–42.
Kessler, J.D., Valentine, D.L., Redmond, M.C., Mengran, D., Chan, E.W., Mendes, S.D., Quiroz, E.W., Villanueva, C.J., Shusta, S.S., Werra, L.M., Yvon-Lewis, S.A., Weber, T.C., 2011. A persistent oxygen anomaly reveals the fate of spilled methane in the deep gulf of Mexico. Science 331 (6015), 312–315.
King, L.H., MacLean, B., 1970. Pockmarks on the Scotian shelf. Geol. Soc. Am. Bull. 81, 3141–3148.
Klaucke, I., Masson, D.G., Petersen, C.J., Weinrebe, W., Ranero, C.R., 2008. Multifrequency geoacoustic imaging of fluid escape structures offshore Costa Rica: implications for the quantification of seep processes. Geochem. Geophys. Geosyst. 9 (4).
Kopf, A.J., 2002. Significance of mud volcanism. Rev. Geophys. 40 (2–1), 2–52.
Körber, J.H., Sahling, H., Pape, T., dos Santos Ferreira, C., MacDonald, I., Bohrmann, G., 2014. Natural oil seepage at Kobuleti Ridge, eastern Black Sea. Mar. Pet. Geol. 50, 68–82.
Kort, E.A., Frankenberg, C., Costigan, K.R., Lindenmaier, R., Dubey, M.K., Wunch, D., 2014. Four corners: the largest US methane anomaly viewed from space. Geophys. Res. Lett. 41 (19), 6898–6903.
Kvenvolden, K.A., Rogers, B.W., 2005. Gaia's breath—global methane exhalations. Mar. Pet. Geol. 22, 579–590.
Langseth, M.G., Westbrook, G.K., Hobart, M.A., 1988. Geophysical survey of a mud volcano seaward of the Barbados Ridge Accretionary Complex. J. Geophys. Res. Solid Earth 93, 1049–1061.
Lee, K.-I.I., Choi, B.-K., Yoon, S.-W., 2001. Acoustic pressure reflection coefficients of a subsurface bubble layer in water. J. Korean Phys. Soc. 40, 256–263.
Leifer, I., MacDonald, I., 2003. Dynamics of the gas flux from shallow gas hydrate deposits: interaction between oily hydrate bubbles and the oceanic environment. Earth Planet. Sci. Lett. 210, 411–424.
Leifer, I., Boles, J., Luyendyk, B., Clark, J., 2004. Transient discharges from marine hydrocarbon seeps: spatial and temporal variability. Environ. Geol. 46, 1038–1052.
Linke, P., Sommer, S., Rovelli, L., McGinnis, D., 2010. Physical limitations of dissolved methane fluxes: the role of bottom layer processes. Mar. Geol. 272, 209–222.
Lister, C.R.B., 1980. Heat flow and hydrothermal circulation. Annu. Rev. Earth Planet. Sci. 8, 95–117.
Løseth, H., Gading, M., Wensaas, L., 2009. Hydrocarbon leakage interpreted on seismic data. Mar. Pet. Geol. 26, 1304–1319.
Løseth, H., Wensaas, L., Arntsen, B., Hanken, N.-M., Basire, C., Graue, K., 2011. 1000 m long gas blow-out pipes. Mar. Pet. Geol. 28, 1047–1060.
Maini, B.B., Bishnoi, P., 1981. Experimental investigation of hydrate formation behaviour of a natural gas bubble in a simulated deep sea environment. Chem. Eng. Sci. 36, 183–189.
Marcelle-De Silva, J., Thomas, A., De Landro Clarke, W.L., Allum, M., 2012. Evidence of gas hydrates in block 26—offshore Trinidad. Energies 5, 1309–1320.
Marques, C.R., Clarke, J.E.H., 2012. Automatic mid-water target tracking using multibeam water column. In: Canadian Hydrographic Conference, Niagara Falls.
Martin, J.B., Kastner, M., Henry, P., Le Pichon, X., Lallement, S., 1996. Chemical and isotopic evidence for sources of fluids in a mud volcano field seaward of the Barbados accretionary wedge. J. Geophys. Res. Solid Earth 101, 20325–20345.
Max, M.D., 1990. Gas Hydrate and Acoustically Laminated Sediments: Potential Environmental Cause of Anomalously Low Acoustic Bottom Loss in Deep-ocean Sediments. Naval Research Laboratory Report 9235 (available through DTEC), 68 pp.
Max, M.D. (Ed.), 2003. Natural Gas Hydrate in Oceanic and Permafrost Environments, second ed. Kluwer Academic Pub.
Max, M.D., Johnson, A.H., Dillon, W.P., 2006. Economic Geology of Natural Gas Hydrate. Kluwer Academic Pub.
Max, M.D., Clifford, S.M., Johnson, A.H., 2013. Hydrocarbon system analysis for methane hydrate exploration on Mars. In: Ambrose, W.A., Reilly, J.F., Peters, D.C. (Eds.), Energy Resources for Human Settlement in the Solar System and Earth's Future in Space, AAPG Memoir 101, pp. 99–114.
Max, M.D., Johnson, A.H., 2014. Hydrate petroleum system approach to natural gas hydrate exploration. Pet. Geosci. 20, 187–199.
McConnell, D., Gharib, J., Henderson, J., Danque, A., Digby, A., Orange, D., 2008. Multibeam Echosounders and Seismic Data Detect Seeps, Enhancing Hydrocarbon Exploration Potential. World Oil Online.
McGinnis, D.F., Greinert, J., Artemov, Y., Beaubien, S.E., Wüest, A., 2006. Fate of rising methane bubbles in stratified waters: how much methane reaches the atmosphere? J. Geophys. Res. Oceans (1978-2012) 111 (C9), C09007.
McGuire, B., Maslin, M.A., 2012. Climate Forcing of Geological Hazards. Wiley-Blackwell.
Milkov, A., 2000. Worldwide distribution of submarine mud volcanoes and associated gas hydrates. Mar. Geol. 167, 29–42.
Milkov, A.V., 2004. Global estimates of hydrate-bound gas in marine sediments: how much is really out there? Earth Sci. Rev. 66, 183–197.
Moore, G.F., Shipley, T.H., 1988. Behavior of the decollement at the toe of the Middle America Trench. Geol. Rundsch. 77, 275–284.
Murton, B.J., Biggs, J., 2003. Numerical modelling of mud volcanoes and their flows using constraints from the Gulf of Cadiz. Mar. Geol. 195 (1), 223–236.
Naudts, L., Greinert, J., Poort, J., Belza, J., Vangampelaere, E., Boone, D., Linke, P., Henriet, J.-P., De Batist, M., 2010. Active venting sites on the gas-hydrate-bearing Hikurangi Margin, off New Zealand: diffusive-versus bubble-released methane. Mar. Geol. 272, 233–250.
Newman, K.R., Cormier, M.-H., Weissel, J.K., Driscoll, N.W., Kastner, M., Solomon, E.A., Robertson, G., Hill, J.C., Singh, H., Camilli, R., 2008. Active methane venting observed at giant pockmarks along the US mid-Atlantic shelf break. Earth Planet. Sci. Lett. 267, 341–352.
Nikolovska, A., Sahling, H., Bohrmann, G., 2008. Hydroacoustic methodology for detection, localization, and quantification of gas bubbles rising from the seafloor at gas seeps from the eastern Black Sea. Geochem. Geophys. Geosyst. 9, Q10010.
Nisbet, E.G., Dlugokencky, E.J., Bousquet, P., 2014. Methane on the rise—again. Science 343 (6170), 493–495.
Paull, C.K., Ussler, W., Dallimore, S.R., Blasco, S.M., Lorenson, T.D., Melling, H., Medioli, B.E., Nixon, F.M., McLaughlin, F.A., 2007. Origin of pingo-like features on the Beaufort Sea shelf and their possible relationship to decomposing methane gas hydrates. Geophys. Res. Lett. 34 (1), L01603.
Phrampus, B.J., Hornbach, M.J., 2012. Recent changes to the Gulf Stream causing widespread gas hydrate destabilization. Nature 490, 527–530.
Pichot, T., Patriat, M., Westbrook, G., Nalpas, T., Gutscher, M.-A., Roest, W., Deville, É., Moulin, M., Aslanian, D., Rabineau, M., 2012. The Cenozoic tectonostratigraphic evolution of the Barracuda Ridge and Tiburon Rise, at the western end of the North America-South America plate boundary zone. Mar. Geol. 303, 154–171.
Pilcher, R., Argent, J., 2007. Mega-pockmarks and linear pockmark trains on the West African continental margin. Mar. Geol. 244, 15–32.
Plaza-Faverola, A., Johnson, J.E., Chand, S., Knies, J., Mienert, J., Franek, P., Bünz,, S., 2015. Role of tectonic stress in seepage evolution along the gas hydrate charged Vestnesa Ridge, Fram Strait. Geophysical Research Letters 42. http://dx.doi.org/10.1002/2014GL062474.
Pohlman, J.W., Bauer, J., Canuel, E., Grabowski, K., Knies, D., Mitchell, C., Whiticar, M., Coffin, R.B., 2009. Methane sources in gas hydrate-bearing cold seeps: evidence from radiocarbon and stable isotopes. Mar. Chem. 115, 102–109.
Rehder, G., Brewer, P.W., Peltzer, E.T., Friederich, G., 2002. Enhanced lifetime of methane bubble streams within the deep ocean. Geophys. Res. Lett. 29, 1731.
Reid, J., Mantyla, A., 1994. World Ocean Dataset. Available from Scripps Institute of Oceanography: ftp://minerva.ucsd.edu.
Riedel, M., Spence, G.D., Chapman, N.R., Hyndman, R.D., 2002. Seismic investigations of a vent field associated with gas hydrates, offshore Vancouver Island. J. Geophys. Res. Solid Earth 107, 2200.
Roberts, H.H., Hardage, B.A., Shedd, W.W., Hunt Jr., J., 2006. Seafloor reflectivity—an important seismic property for interpreting fluid/gas expulsion geology and the presence of gas hydrate. Lead. Edge 25, 620–628.

Rubino, A., Falcini, F., Zanchettin, D., Bouche, V., Salusti, E., Bensi, M., Riccobene, G., De Bonis, G., Masullo, R., Simeone, F., Piattelli, P., Sapienza, P., Russo, S., Platania, G., Sedita, M., Reina, P., Avolio, R., Randazzo, N., Hainbucher, D., Capone, A., 2012. Abyssal undular vortices in the Eastern Mediterranean basin. Nat. Commun. 3, 834.

Sager, W.W., MacDonald, I.R., Hou, R., 2003. Geophysical signatures of mud mounds at hydrocarbon seeps on the Louisiana continental slope, northern Gulf of Mexico. Mar. Geol. 198, 97–132.

Sager, W.W., Bryant, W.R., Doyle, E.H., 2004a. Introduction: resolution is the solution. AAPG Bull. 88 (6), 699–701.

Sager, W.W., MacDonald, I.R., Hou, R., 2004b. Side-scan sonar imaging of hydrocarbon seeps on the Louisiana continental slope. AAPG Bull. 88, 725–746.

Sahling, H., Masson, D.G., Ranero, C.R., Hühnerbach, V., Weinrebe, W., Klaucke, I., Bürk, D., Brückmann, W., Suess, E., 2008. Fluid seepage at the continental margin offshore Costa Rica and southern Nicaragua. Geochem. Geophys. Geosyst. 9, Q05S05.

Sauter, E.J., Muyakshin, S.I., Charlou, J.-L., Schlüter, M., Boetius, A., Jerosch, K., Damm, E., Foucher, J.-P., Klages, M., 2006. Methane discharge from a deep-sea submarine mud volcano into the upper water column by gas hydrate-coated methane bubbles. Earth Planet. Sci. Lett. 243, 354–365.

Savini, A., Malinverno, E., Etiope, G., Tessarolo, C., Corselli, C., 2009. Shallow seep-related seafloor features along the Malta plateau (Sicily channel–Mediterranean Sea): Morphologies and geo-environmental control of their distribution. Mar. Pet. Geol. 26, 1831–1848.

Schneider, J., Greinert, J., Chapman, N., Rabbel, W., Linke, P., 2010. Acoustic imaging of natural gas seepage in the North Sea: sensing bubbles under control of variable currents. Limnol. Oceanogr. Methods 8, 155–171.

Serié, C., Huuse, M., Schødt, N.H., 2012. Gas hydrate pingoes: deep seafloor evidence of focused fluid flow on continental margins. Geology 40, 207–210.

Shipley, T.H., Houston, M.H., Buffler, R.T., Shaub, F.J., McMillen, K.J., Ladd, J.W., Worzel, J.L., 1979. Seismic evidence for widespread possible gas hydrate horizons on continental slopes and rises. AAPG Bull. 63, 2204–2213.

Simonetti, A., Knapp, J.H., Sleeper, K., Lutken, C.B., Macelloni, L., Knapp, C.C., 2013. Spatial distribution of gas hydrates from high-resolution seismic and core data, Woolsey Mound, Northern Gulf of Mexico. Mar. Pet. Geol. 44, 21–33.

Skarke, A., Ruppel, C., Kodis, M., Brothers, D., Lobecker, E., 2014. Widespread methane leakage from the sea floor on the northern US Atlantic margin. Nat. Geosci. 7, 657–661.

Sloan, E.D., Koh, C.A., 2008. Clathrate Hydrates of Natural Gases. CRC Press LLC.

Smith, A.J., Mienert, J., Bünz, S., Greinert, J., 2014. Thermogenic methane injection via bubble transport into the upper Arctic Ocean from the hydrate-charged Vestnesa Ridge, Svalbard. Geochem. Geophys. Geosyst. 15 (5), 1945–1959.

Solomon, E.A., Kastner, M., MacDonald, I.R., Leifer, I., 2009. Considerable methane fluxes to the atmosphere from hydrocarbon seeps in the Gulf of Mexico. Nat. Geosci. 2, 561–565.

Spahni, R., Chappellaz, J., Stocker, T.F., Loulergue, L., Hausammann, G., Kawamura, K., Flückiger, J., Schwander, J., Raynaud, D., Masson-Delmotte, V., Jouzel, J., 2005. Atmospheric methane and nitrous oxide of the late Pleistocene from Antarctic ice cores. Science 310 (5752), 1317–1321.

Talukder, A.R., Bialas, J., Klaeschen, D., Buerk, D., Brueckmann, W., Reston, T., Breitzke, M., 2007. High-resolution, deep tow, multichannel seismic and side-scan sonar survey of the submarine mounds and associated BSR off Nicaragua pacific margin. Mar. Geol. 241, 33–43.

Talukder, A.R., 2012. Review of submarine cold seep plumbing systems: leakage to seepage and venting. Terra Nova 24, 255–272.

Tinivella, U., Giustiniani, M., 2012. An overview of mud volcanoes associated to gas hydrate system. In: Nemeth, K. (Ed.), Updates in Volcanology - New Advances in Understanding Volcanic Systems. InTech, Rijeka, pp. 225–267.

Tomczak, M., Haffner, G.D., Fronaes, E., 2002. False-bottom acoustic echo in mid water? A note on how to evaluate and prevent the interference. IEEE J. Ocean. Eng. 27 (4), 870–872.

Torres, M., McManus, J., Hammond, D., De Angelis, M., Heeschen, K., Colbert, S., Tryon, M., Brown, K., Suess, E., 2002. Fluid and chemical fluxes in and out of sediments hosting methane hydrate deposits on Hydrate Ridge, OR, I: hydrological provinces. Earth Planet. Sci. Lett. 201, 525–540.

Tryon, M.D., Brown, K.M., Torres, M.E., Tréhu, A.M., McManus, J., Collier, R.W., 1999. Measurements of transience and downward fluid flow near episodic methane gas vents, Hydrate Ridge. Cascadia Geol. 27, 1075–1078.

Tryon, M.D., Brown, K.M., Torres, M.E., 2002. Fluid and chemical flux in and out of sediments hosting methane hydrate deposits on Hydrate Ridge, OR, II: hydrological processes. Earth Planet. Sci. Lett. 201, 541–557.

Van Dover, C., Aharon, P., Bernhard, J., Caylor, E., Doerries, M., Flickinger, W., Gilhooly, W., Goffredi, S., Knick, K., Macko, S., 2003. Blake Ridge methane seeps: characterization of a soft-sediment, chemosynthetically based ecosystem. Deep Sea Res. I Oceanogr. Res. Pap. 50, 281–300.

Van Rensbergen, P., De Batist, M., Klerkx, J., Hus, R., Poort, J., Vanneste, M., Granin, N., Khlystov, O., Krinitsky, P., 2002. Sublacustrine mud volcanoes and methane seeps caused by dissociation of gas hydrates in Lake Baikal. Geology 30, 631–634.

Walsh, J.J., Nicol, A., Childs, C., 2002. An alternative model for the growth of faults. J. Struct. Geol. 24, 1669–1675.

Warzinski, R.P., Lynn, R., Haljasmaa, I., Leifer, I., Shaffer, F., Anderson, B.J., Levine, J.S., 2014. Dynamic morphology of gas hydrate on a methane bubble in water: observations and new insights for hydrate film models. Geophys. Res. Lett. 41 (19), 6841–6847.

Weber, T.C., De Robertis, A., Greenaway, S.F., Smith, S., Mayer, L., Rice, G., 2012. Estimating oil concentration and flow rate with calibrated vessel-mounted acoustic echo sounders. Proc. Natl. Acad. Sci. 109, 20240–20245.

Weber, T.C., Mayer, L., Jerram, K., Beaudoin, J., Rzhanov, Y., Lovalvo, D., 2014. Acoustic estimates of methane gas flux from the seabed in a 6000 km2 region in the Northern Gulf of Mexico. Geochem. Geophys. Geosyst. 15, 1911–1925.

Westbrook, G., Smith, M., 1983. Long decollements and mud volcanoes: evidence from the Barbados Ridge Complex for the role of high pore-fluid pressure in the development of an accretionary complex. Geology 11, 279–283.

Westbrook, G., Mascle, A., Biju-Duval, B., 1984. Geophysics and structure of the Lesser Antilles forearc. Initial Reports Deep Sea Drilling Program, LXXVIIIA, pp. 23–38.

Wynn, R.B., Huvenne, V.A., Le Bas, T.P., Murton, B.J., Connelly, D.P., Bett, B.J., Ruhl, H.A., Morris, K.J., Peakall, J., Parsons, D.R., Sumner, E.J., Darby, S.E., Dorrell, R.M., Hunt, J.E., 2014. Autonomous Underwater Vehicles (AUVs): their past, present and future contributions to the advancement of marine geoscience. Mar. Geol. 352, 451–468.

Zemskaya, T.I., Sitnikova, T.Y., Kiyashko, S.I., Kalmychkov, G.V., Pogodaeva, T.V., Mekhanikova, I.V., Naumova, T.V., Shubenkova, O.V., Chernitsina, S.M., Kotsar, O.V., 2012. Faunal communities at sites of gas-and oil-bearing fluids in Lake Baikal. Geo-Mar. Lett. 32, 437–451.

Zitter, T.A.C., Huguen, C., Woodside, J.M., 2005. Geology of mud volcanoes in the eastern Mediterranean from combined sidescan sonar and submersible surveys. Deep Sea Res. I Oceanogr. Res. Pap. 52, 457–475.